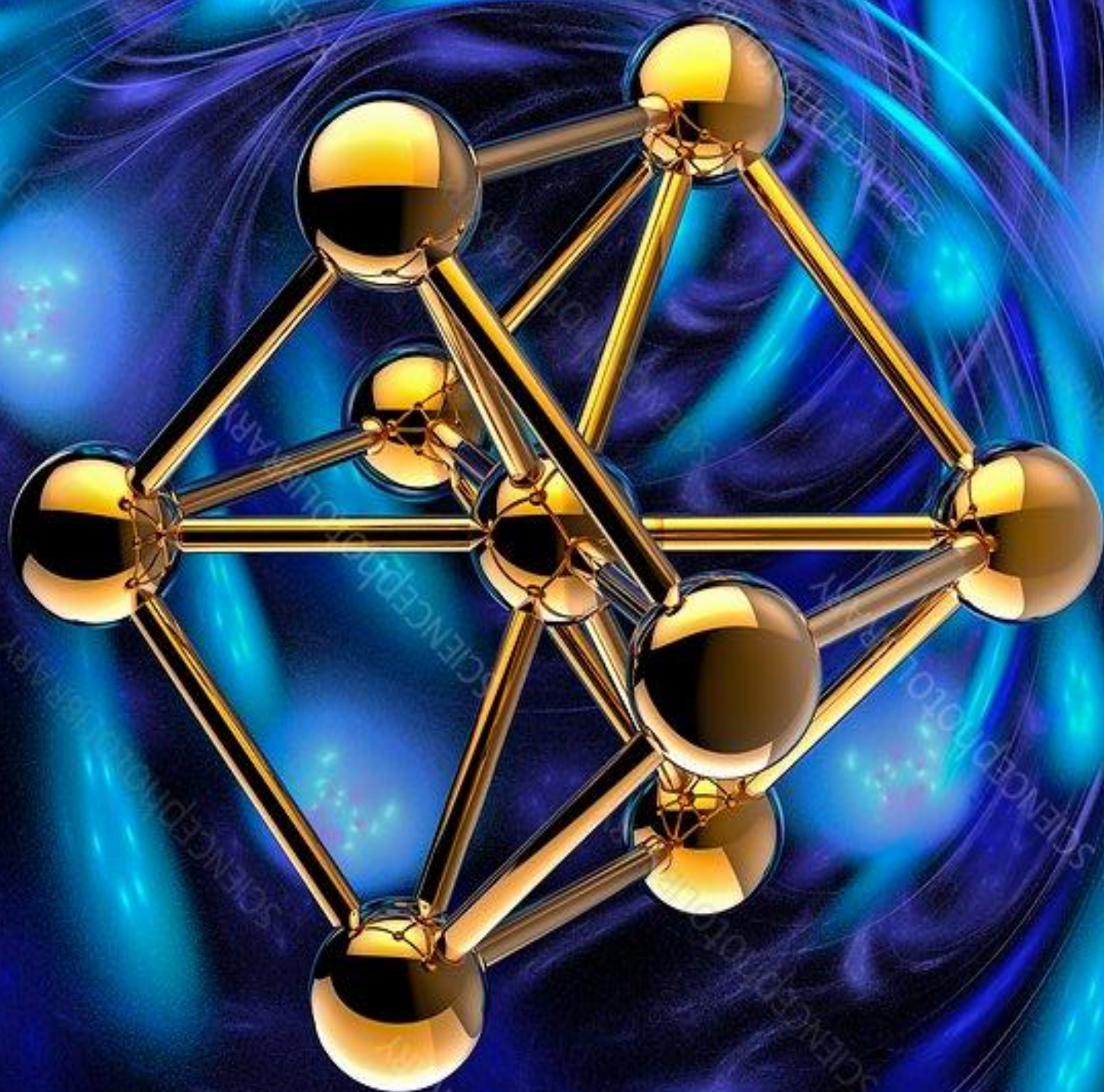


**SYNTHESIS, CHARACTERIZATION,  
SOLID-STATE STUDIES  
&  
APPLICATIONS OF  
NICKEL-ZINC FERRITES**



**SYNTHESIS, CHARACTERIZATION, SOLID-STATE STUDIES**  
**AND APPLICATIONS OF NICKEL-ZINC FERRITES**

A project report submitted to

**GOA UNIVERSITY**

In partial fulfilment of the requirements for the degree of  
**MASTER OF SCIENCE IN CHEMISTRY**

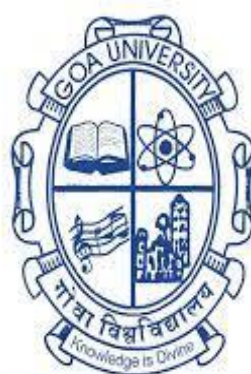
BY

**Ms. Sweta Santosh Thakkarkar**

**Reg No. 20P0490091**

Under the Guidance of

**Prof. Dr. Vidhyadatta M. S. Verenkar**



**GOA UNIVERSITY**  
गोंय विद्यापीठ

**SCHOOL OF CHEMICAL SCIENCES**  
**GOA UNIVERSITY, TALEIGAO, PANAJI-GOA**  
**2021-2022**

**CERTIFICATE**

This is to certify that the dissertation entitled “**Synthesis, Characterization, solid state studies & Applications Nickel-Zinc Ferrites**” is bonafied work carried out by Ms. Sweta Santosh Thakkarkar under my supervision in partial fulfilment of the requirement for the award of the degree of Master of Science at School of Chemical Sciences, Goa University.

**Prof. Dr. Vidhyadatta M. S. Verenkar**

**Project Guide  
Dean  
School of Chemical Sciences  
Goa University**

## **DECLARATION**

I hereby declare that embodied in this report entitled “Synthesis, Characterization, solid state studies & Applications Nickel-Zinc Ferrites” was carried out by me during the year 2021-2022 under the guidance of Prof. Dr. Vidhyadatta Verenkar. In keeping with the general practices of reporting scientific observations, due to acknowledgements have been made whatever the work described is based on the findings of other investigators.

**SWETA SANTOSH THAKKARKAR**

**M. Sc Part II, Inorganic Chemistry**

**School of Chemical Sciences**

**Goa University**

## **ACKNOWLEDGEMENT**

First and foremost, I would like to thank God who has given me the power to believe in myself and pursuing my dreams. His unending showers of blessings helped me to complete my work successfully.

I take immense pleasure to express my sincere and deep sense of gratitude to my supervising guide Prof. Dr. Vidhyadatta Verenkar for his sustained enthusiasm and positivity throughout the course of my project work. It was a grate privilege and honour to work and study under his guidance.

I wish to express my hearty thanks to my colleagues. I am extremely grateful to my parents for their love, prayers, caring and sacrifices for educating and preparing me for my future.

**SWETA SANTOSH THAKKARKAR**

## INDEX

<b>Sr.No</b>	<b>TITLE</b>	<b>Page No.</b>
<b>01.</b>	<b>Introduction</b>	<b>01</b>
1.1	Ferrites	<b>01</b>
1.2	Classification of ferrites	<b>02</b>
1.3	Spinel ferrites	<b>02</b>
1.4	History of ferrites	<b>03</b>
1.5	Ni-Zn ferrites	<b>05</b>
<b>02.</b>	<b>Literature review</b>	<b>06</b>
2.2	Experimental methods of preparation, characterisation & Solid-state studies	<b>06-20</b>
2.3	<b>Applications</b>	<b>21</b>
<b>03.</b>	<b>Conclusion</b>	<b>22</b>
<b>04.</b>	<b>References</b>	<b>23-30</b>

# **1. INTRODUCTION**

## **1.1 FERRITES**

The term “**ferrite**” is derived from the Latin word “**Ferrum**,” meaning iron. Ferrites are ceramic ferromagnetic materials, which are mainly composed of ferric oxide,  $\alpha$ -Fe<sub>2</sub>O<sub>3</sub>, in a large proportion that is mixed with a metallic element such as barium, manganese, nickel, zinc in small proportions. The molecular formula of ferrites is  $M^{2+}OFe_2^{3+}O_3$ , where M stands for the divalent metal such as Fe, Mn, Cu, Co, Zn, Ni, Mg, etc<sup>1,2</sup>.

The term ferrite is generally used to describe a family of magnetic oxide compounds containing iron oxide as the main component<sup>1,2</sup>. Ferrites, in general can adopt three different crystal lattices namely spinel ferrites (cubic), hexaferrites (hexagonal) and garnets (cubic). Each of these structures give rise to magnetic properties which in turn may change with the chemical composition and ordering of the ions in the crystal lattice. The spinel ferrites have a general formula of AB<sub>2</sub>O<sub>4</sub><sup>2</sup>. Spinel ferrites generally contain two cation sites for metal cation occupancy. There are eight A sites where the metal cations are tetrahedrally coordinated by oxygen and sixteen B sites with octahedral coordination. It is important to know that when A sites are occupied by M<sup>+2</sup> cations and B sites are occupied by Fe<sup>+3</sup> cations, the ferrite structure is that of normal spinel<sup>3</sup>. On the other hand, when A sites are occupied by trivalent metal ions i.e., Fe<sup>+3</sup> and B site possesses both the divalent (M<sup>+2</sup>) and trivalent ions (Fe<sup>+3</sup>), the ferrite structure is that of inverse spinel<sup>4</sup>. However, in most spinels the cation distribution possesses an intermediate degree of inversion wherein both sites contain a fraction of the M<sup>+2</sup> and Fe<sup>+3</sup> cations<sup>3</sup>.

They are extensively studied due to their unique magnetic properties. The academic interest in the study of ferrites is because they are the most important electronic and magnetic ceramics. The structural, optical, magnetic, electrical and electromagnetic property of ferrites depends on the method of preparation, sintering temperature, sintering rate, sintering duration, and sintering atmosphere. There are various methods used for the preparation of ferrites such as Co-precipitation, sol-gel method, and hydrothermal method. The magnetic nanoparticles (MNPs) have gained a significant importance because of their applications in a variety of disciplines such as medical application like biomedicine, magnetic resonance imaging, Catalysis, gas sensors, etc. Various methods have been employed for the preparation of these compounds like solid state reaction, sol-gel method, self-propagating high temperature synthesis, solvothermal method, etc

The potential applications of ferrites in electronics, microwave, and computer technologies have focused the attention of many research workers on these materials.

## **1.2 CLASSIFICATION OF FERRITES**

**Ferrites are classified on the basis of magnetic properties and crystal structure.** On the basis of the ability to be magnetized and demagnetized, ferrites are classified as **soft ferrites** and **hard ferrites**.

Hard ferrites have a high coercivity and such materials are difficult to magnetize. Therefore, these materials are used in making permanent magnets which are used for applications in the refrigerator, washing machine, communication systems, switch-mode power supplies, dc-dc converters, microwave absorbing systems, high-frequency applications, etc<sup>3</sup>.

On the other hand, soft ferrites have low coercivity as a result of which their magnetization can easily be altered. Soft ferrites are good conductors of the magnetic field which has led to their wide range of applications in the electronic industry such as developing transformer cores, high-frequency inductors, and microwave components<sup>3</sup>. Mn-Zn, Mg-Zn, Ni-Zn ferrite are the example of soft ferrite.

Based on crystal structure there are four important classes of ferrite such as **spinel**, **garnet**, **hexagonal**, and **ortho** ferrite<sup>3</sup>. Of which spinel class is considered as important because of its stability compared to other ferrites and also because many commercially available ferrites have this crystal structure. Ferrite nanoparticles with a spinel structure have received considerable attention in the field of nanoelectronics. These materials are used as deflection yoke rings, computer memory chips, microwave devices, transducers and transformers due to their high electrical resistivity, high permeability and saturation magnetization<sup>4</sup>.

## **1.3 SPINEL FERRITES**

**Spinel ferrites** are soft magnets which find application in microwave devices and transformers<sup>5</sup>. The spinel ferrite nanoparticles have grown significant consideration from the last few decades due to their superparamagnetic behaviour, low melting point, high saturation magnetization, and low coercivity. Among the various nanoparticles used in the field including Medical Science, the spinel ferrites are the subject of research due to its extensive range of applications viz. humidity sensors, biosensors, magnetic storage systems, magnetic recording media, microwave devices, noise filters, magnetocaloric refrigeration, transformer cores, gas

sensors, drug delivery, ferrofluids, magnetic resonance imaging, hyperthermia, etc. The above applications of spinel ferrites are because of its ferrimagnetic and semiconductor properties. The ferrimagnetic materials are categorized as a subclass of magnetic materials. In these materials, the magnetic moment of unequal magnitude has aligned in the opposite direction<sup>6</sup>. The spinel ferrites have the common formula as  $MFe_2O_4$ , where M may be any divalent metal ion ( $Mn^{2+}$ ,  $Mg^{2+}$ ,  $Zn^{2+}$ ,  $Co^{2+}$ ,  $Ni^{2+}$ , and  $Cu^{2+}$ )<sup>6</sup>.

The spinel structure presents two types of crystal sites where the cations  $Me^{2+}$  and  $Fe^{3+}$  can be distributed tetrahedral sites (A sites) and octahedral sites (B sites). Typically, two extreme types of spinel structure are favorable: normal spinel and inverse spinel, but in practice mixed spinel structure are also observed. In normal spinel structure, the A sites are taken by the  $Me^{2+}$  and the B sites are occupied by the  $Fe^{3+}$  cations. In inverse spinel structure, the  $Fe^{3+}$  cations are distributed between the A and B sites and octahedral sites and the  $Me^{2+}$  cations are found in B sites. The mixed spinel structure has the cations distributed in a combined mode between the normal and inverse structure. The magnetic and electric properties of the soft ferrite are closely associated with their intracrystalline ordering of the cations<sup>7</sup>.

#### **1.4 HISTORY OF FERRITES**

The first systematic study on the relationship between chemical composition and magnetic properties of various ferrites was reported by Hilpert in 1909. At that time, Hilpert had successfully prepared spinel ferrites, such as manganese, copper, cobalt, magnesium, and zinc. After that many researchers have worked on ferrites to find new ferrites with specific electrical and magnetic properties. **Yogoro Kato and Takeshi Takei of the Tokyo Institute of Technology synthesized the first ferrite compounds in 1930.** Since 1930, Japan and the Netherlands have started researching soft ferrites. However, it was in the year 1945 that J.L. Snoek of the Philips Research Laboratories in the Netherlands successfully synthesized soft ferrites for commercial applications. The mechanism for the enhancement of magnetization (ferromagnetism) by the addition of zinc ferrite was explained successfully by Neel of France in 1948. Barium hexaferrite ( $BaO \cdot 6Fe_2O_3$ ) was discovered in 1950 at Philips Physics Laboratory and was an accidental discovery.

Our modern telecommunication system would not be possible without ferrites. The largescale production of television in the 1950s was the main reason for the expansion of the ferrite industry. Steward started producing hard ferrites which are used in the automotive industry

whereas soft ferrites deflection yokes for TV. In 1952, Philips researchers prepared Ni-Zn and Mn-Zn ferrite for use in TV tube deflection yokes and high voltage flyback transformers. The invention of hexagonal ferrite magnets such as the barium and strontium ferrite magnet by Went *et al.* in 1952 or the completion of ferroplanna-type hexagonal ferrites by Jonker *et al.* in 1957 is also considered a very important event in the history of ferrites. In the 1960s Philips developed strontium hexaferrite ( $\text{SrO} \cdot 6\text{Fe}_2\text{O}_3$ ), with better properties than barium hexaferrite. Other materials also develop with improved properties such as  $\text{BaO} \cdot 2(\text{FeO}) \cdot 8(\text{Fe}_2\text{O}_3)$  came in 1980 and  $\text{Ba}_2\text{ZnFe}_{18}\text{O}_{23}$  came in 1991.

**The first commercial soft ferrite product in Korea was radio antenna core in 1970.** Goldman in 1975 produced Ni-Zn ferrites for microwave application. In 1976, Samwha electronics Co. Ltd prepared high-quality soft ferrite for use in new technology. In the era of 1950 to 1970, approximately 20 years steward become a supremo producer of ferrite in both hard, soft ferrite and also in materials having application in telecommunications, electronics, copiers, military, and automotive industries. In the year 1995, composites based on nano-sized magnetic materials were reported for high-density information storage, Ferro-fluids, and medical diagnosis. After 1996 new methods to prepare fine particles of ferrites were used. Prominent among them are Coprecipitation, sol-gel synthesis, Freeze-drying, hydrothermal oxidation, activated sintering, organic precursors, and decomposition process. Various ICF's (International Conference on Ferrites) that providing a forum for exchanging information on the science and technology of ferrites and related materials have taken place from 1970 to 2000. In the 1990s ferrites were used as noise filters in power lines on the input to all types of electronic equipment. Ferrite was investigated to be used as a magnetic carrier for electro-photography. After 2000, research into the synthesis and characterization of nano-structured systems has exploded. The Properties of nano-scale material often differ considerably from their bulk phase material. The ICF held between 2004-2013 made focus on the latest science, technology, and application of ferrites<sup>1,2</sup>.

N Jiang et al. studied the influence of zinc concentration on various properties of as prepared Ni-Zn ferrites prepared by solid state reaction method. The lattice parameter was reported to increase from 8.354 Å to 8.452 Å as the zinc concentration was increased. The magnetic permeability  $\mu'$  decreased in an external magnetic field and showed two resonance peaks corresponding to domain wall and spin rotation resonance. The values  $\epsilon'$  and  $\epsilon''$  decreased with increasing frequency until they reach almost constant in 3MHz to 1GHz range. The spinel

ferrites  $MZn_xFe_2O_4$  ( $x=0.2, 0.5$  and  $0.8$ ) were synthesized by sol-gel combustion method by W. Wang et al. [12] and further fabricated by mixing with epoxy resin to study microwave absorbing property. The microstructure and surface morphology of this ferrites were studied by XRD and SEM techniques. The complex permittivity and complex permeability of composites were also investigated. G. Datt et al. prepared nickel cobalt ferrite by solvothermal method. They used various techniques to study and characterize their samples like XRD, electron microscopy and Mossbauer spectroscopy They reported that this material can be in future be used in spintronics, magneto-electronics, and ultra-high-density recording media as well as for radar absorbing applications. Among the soft magnetic materials, Ni-Zn ferrites have received special attention because of their good magnetic properties and high electric resistivity over a wide range of frequencies but they did show low permeability.

### 1.5 Ni-Zn FERRITES

Soft magnetic Ni-Zn ferrite nanoparticles have essential need for the high frequency applications due to the high electrical DC resistivity, high saturation magnetization and high magnetic permeability. The surface to volume ratio of these nano-materials is very large as compared to the bulk counterparts that influences their properties like spin canting, surface anisotropy, super-paramagnetism<sup>64-78</sup>. Ni ferrite has an inverse spinel structure while Zn is known to have normal spinel structure but the composite Ni-Zn ferrites are known as mixed spinel structure. In zinc ferrite, zinc is diamagnetic in nature; in nickel ferrite, nickel is ferromagnetic in nature. As a whole, the net magnetic moment in spinel ferrite is decided by metal ions occupying A and B sites. In Nickel-Zinc ferrites, zinc ions occupy A-sites and Nickel ions occupy B- sites along with ferromagnetic iron ions resulting in a maximum magnetic moment making these Ni-Zn ferrites usable for multiple applications. Nickel–zinc ferrites are soft ferrimagnetic materials having low magnetic coercivity, low dielectric constant, high corrosion resistance, extremely high resistivity, high permeability and little eddy-current loss in the high frequency range. Microstructure and magnetic properties of these ferrites are highly sensitive to the preparation methodology, sintering conditions and the amount of constituent metal oxides, impurities or doping levels.

## 2. LITERATURE REVIEW

### 2.1 EXPERIMENTAL METHODS OF PREPARATION, CHARACTERISATION & SOLID-STATE STUDIES

Several synthesis methods can be used to obtain cobalt-nickel ferrites as reported in the literature including sol-gel, co-precipitation, hydrothermal, mechano-chemical, refluxing, precursor, microwave processing, sol-gel auto-combustion, etc<sup>8,9</sup>. Some of the most commonly used experimental methods of preparation mentioned in the literature are discussed below:

Pooja Dhiman et al.<sup>10</sup> synthesized  $\text{Ni}_{1-x}\text{Zn}_x\text{Fe}_2\text{O}_4$  ( $x = 0.0, 0.1, 0.3, \& 0.5$ ) using the solution combustion method. All chemicals of high purity were utilized for the synthesis. As prepared samples were characterized for phase identification using X-ray diffraction (XRD) and Reitveld refined pattern confirms the formation of single phased cubic structure with a nano-metric crystallite size. The electrical and magnetic properties of synthesized ferrites were studied in detail. The LEV removal rate was substantially in presence of persulfate ( $k_{\text{app}} = 0.08563 \text{ min}^{-1}$ ) and hydrogen peroxide ( $k_{\text{app}} = 0.07966 \text{ min}^{-1}$ ). The homogeneous distribution of grains and particles is evidenced by shape and size morphological studies. Raman spectroscopy reveals the presence of motion of oxygen in tetrahedral and octahedral voids. The dc electrical resistivity measured using the two-probe method is found to be in the range of  $10^7$  to  $10^8 \Omega \text{ cm}$ . The optical band gap measured for all photo-catalysts resides at 2.11–2.53 eV. The ferrite photocatalyst exhibits high visible absorption, superior charge transfer capacity, and highly suppressed recombination as suggested by electrochemical impedance spectroscopy and photoluminescence results. The change in band structure with variable Zn content was monitored by shifting of conduction and valence bands. The optical absorption, electrochemical impedance spectroscopy and photoluminescence results suggest that  $\text{Ni}_{0.7}\text{Zn}_{0.3}\text{Fe}_2\text{O}_4$  ( $\text{N}_2$ ) has high visible absorption, high charge transfer capacity and diminished electron-hole recombination. This is manifested in superior photo-catalytic LEV degradation of 96.8% under visible light. The degradation was tested by varying various operational parameters, as pH, catalyst dosage, electrolytes and water matrix. In addition, the high photo-activity is achieved under solar light and in tap water and river water. Furthermore, the high magnetic character of the catalysts aids in their retrieval post utilization in catalysis. In terms of band structure analysis, role of dopants, metal redox, and scavenging studies, a suitable photo-catalytic process was proposed. Degradation intermediates discovered by liquid chromatography–mass spectrometry analysis were also recommended as a pathway of degradation. These findings open up exciting possibilities for developing novel solar active photo-catalytic systems based on spinel ferrites for efficient environmental cleanup.

Hua Su et al.<sup>11</sup> synthesized Polycrystalline Ni–Zn ferrite samples with different microstructures by the conventional ceramic technique using AR grade  $\text{Fe}_2\text{O}_3$ , ZnO, CuO, and NiO as raw materials, and their complex permeability and permittivity spectra have been studied. The

permeability spectra have been resolved into contributions of domain wall resonance and spin rotation relaxation. The fitting results of permeability dispersion have revealed the relationships between domain wall resonance, spin rotation relaxation mechanisms, and microstructures. With increasing average grain size, the permittivity also gradually increased. Permittivity also increases with increasing average grain size, which may be ascribed to both an increase in the  $\text{Fe}^{2+}$  concentration and an increase in the grain to grain boundary thickness ratio. However, extremely big grain size led to an uneven permittivity–frequency curve. These results may be rationalized in terms of the modifications of the microstructures brought about by the different sintering temperatures.

Susana M. Olhero et al.<sup>12</sup> synthesized a Ni–Zn ferrite precursor powder by co-precipitation method upon adding ammonia to an aqueous solution of the precursor iron, nickel, and zinc nitrate salts. The powder was calcined at a range of temperatures (200–1200 °C) and the crystalline phase evolution was assessed by X-ray diffraction coupled with Rietveld refinement. Intermediate phases ( $\text{NiFe}_2\text{O}_4$  and  $\text{Fe}_2\text{O}_3$ ) with increasing crystallinity coexisted in the system up to 1000 °C. The required  $\text{Ni}_{0.8}\text{Zn}_{0.2}\text{Fe}_2\text{O}_4$  phase could only be attained at 1200 °C. The magnetic properties measured using a vibrating sample magnetometer revealed high magnetization saturation level ( $\sim 59$  emu/gm) above 400 °C. The mild milling conditions used were not expected to influence the crystalline phase assemblage, although the apparent phase fractions were different, probably due to the lack of homogenization in a kind of core–shell structure induced by the contact with air atmosphere. Moreover, wet milling is more efficient in reducing particle size than hand deagglomeration in a mortar. Using a nitrogen atmosphere has no significant variations in the amount of phases formed. The coercivity showed a steady decrease with increasing heat treatment temperature, leading to a change from a hard to soft magnetic state. The BET specific surface area and the SEM morphology were found to be dependent on calcination temperature, atmosphere (air or  $\text{N}_2$ ) and on the milling procedure.

Nan-Nan Jiang et al.<sup>13</sup> synthesized Polycrystalline soft magnetic nickel–zinc ferrites with chemical composition  $\text{Ni}_{1-x}\text{Zn}_x\text{Fe}_2\text{O}_4$ , where  $x = 0, 0.2, 0.4, 0.6, 0.65, 0.7, 0.75,$  and  $0.8$ , by solid state reaction method. They researched the effect of zinc concentration on the lattice parameter, crystal morphology and electromagnetic properties at high frequency. Results show that  $\epsilon'$  and  $\epsilon''$  decline with increasing frequency until they reach almost constants over 3 MHz to 1 GHz. The dielectric constant achieves a maximum when the Zn concentration is 0.8. The value of  $\epsilon'$  slightly declines with increasing frequency in the range of 2–18 GHz. The spectra of the permeability displays a relaxation resonance for the ferrites with  $x=0, 0.2,$  and  $0.4$  in 3 MHz to 1 GHz frequency range. The permeability is ruled by Snoek's law, which results in the values of  $\mu'$  decreased fast below 2 GHz and smaller than 1 above 2 GHz. The value of  $\mu'$  reaches maximum and  $\mu''$  shows minimum for the samples around  $x=0.75$  in 2–18 GHz range. The magnetic permeability  $\mu'$  decreases in an external magnetic field, and shows two resonance peaks corresponding to domain wall and spin rotation resonance. The resonance peaks shift to higher frequency with increasing the external magnetic field. But the permeability has no clear response for magnetic field when zinc concentration is much higher. T.J. Shinde et al.<sup>14</sup> synthesized Nanocrystalline spinel ferrites with general formula  $\text{Ni}_{1-x}\text{Zn}_x\text{Fe}_2\text{O}_4$  ( $x = 0 - 1.0$ ) by an oxalate co-precipitation method. Analytical grade nickel sulfate, zinc sulfate and ferrous

sulfate were used as starting materials in stoichiometric proportions. Magnetic properties were investigated by means of saturation magnetization, AC susceptibility, cation distribution and Curie temperature measurements. The saturation magnetization increases with increasing concentration of zinc up to  $x=0.4$  and then decreases with increasing zinc concentration. Investigation of the Yafet–Kittel (Y–K) angles shows the existence of Neel’s two sublattice model for  $x \leq 0.2$  and Y–K model for  $x \geq 0.4$  compositions. Variation of normalized AC susceptibility with temperature shows single domain particle nature for the compositions  $x \leq 0.2$ , whereas multi-domain particle nature for the compositions  $x \geq 0.4$ . Curie temperatures of the samples decrease with the increase in zinc concentration. Upadhayay’s model is used to investigate the cation distribution and hence to calculate the Curie temperature. The composition for  $x=1$  shows paramagnetic behavior at and above room temperature. The saturation magnetization and Curie temperature are found to be improved in comparison with sample prepared by the ceramic method and hence make these ferrites useful in electronic devices over a wider frequency range.

M. Jalaly et al.<sup>15</sup> synthesized Nanocrystalline Ni–Zn ferrite ( $\text{NiZnFe}_2\text{O}_4$ ) by high energy ball milling of stoichiometric mixture of ZnO, NiO,  $\text{Fe}_2\text{O}_3$  powders. X-ray powder diffractometry (XRD), scanning electron microscopy (SEM), simultaneous thermal analysing (STA), Fourier transform infrared spectroscopy (FTIR) and vibrating sample magnetometer (VSM) were carried out to characterize the structural, chemical and magnetic aspects of  $\text{NiZnFe}_2\text{O}_4$  compound. The XRD and DSC results showed that mechanism of formation of Ni–Zn ferrite consisted of two stages, the formation of Zn ferrite followed by the dissolution of NiO in Zn ferrite to form Ni–Zn ferrite. The crystallite size of final product after 60 h of ball milling time was estimated to be 18 nm which increased to 45 nm after annealing at 800 °C for 4 h. After annealing the saturation magnetization increased and coercive field decreased due to a reduction in density of lattice defects and corresponding internal strain.

Ch. Srinivas et al.<sup>16</sup> Studied structural, vibrational, elastic and magnetic properties of uniaxial anisotropic Ni-Zn nanoferrites. Co-precipitation method was adopted to obtain zinc ferrite nanoparticles substituted with nickel ( $0.5 \leq x \leq 0.7$ ) followed by sintering at 500 °C for 2 h. The formation of spinel ferrite phase in the present ferrite compositions was confirmed from the X-ray diffractograms. In the existing ferrite systems, the pure ferrite phase was successfully achieved. Due to cation redistribution in ferrite samples, a difference of 1.6–2% between experimental and theoretical parameter is predicted. The experimental lattice parameter ( $a$ ) and average crystallite size ( $\langle D_{\text{XRD}} \rangle$ ) are in between 8.359 - 8.348 Å and 12.8 – 14.9 nm. As doping level of  $\text{Ni}^{2+}$  increases, an interesting relation was existed in between  $a$  and  $\langle D_{\text{XRD}} \rangle$ , such that the first one is decreasing and the later one is increasing. The growth of crystallite size for substitution of smaller  $\text{Ni}^{2+}$  (0.69 Å) showed the thermodynamical stability of ferrite compositions. The variation of average particle size ( $\langle D_{\text{FE-SEM}} \rangle$ ) from FE-SEM is different from the variation of  $\langle D_{\text{XRD}} \rangle$ . The present spinel ferrite  $\text{Ni}_{0.6}\text{Zn}_{0.4}\text{Fe}_2\text{O}_4$  possessed smaller particle size of 17.6 nm. The existence of higher and lower vibrational frequencies in between 579–587  $\text{cm}^{-1}$  and 380–386  $\text{cm}^{-1}$ , satisfied the Waldron proposals for the ferrite phase. The saturation magnetization (MS) at room temperature (RT) has uneven variation and

a highest value of 43.2 emu/g was noticed for the composition  $x = 0.6$ . The coercivity (HC) at RT is gradually increasing with the doping level of  $\text{Ni}^{2+}$  ion incorporation. As temperature is decreasing below the room temperature both the MS and HC are increasing for a particular composition. A.C.F.M. Costa et al.<sup>17</sup> carried out Synthesis and studied microstructure and magnetic properties of Ni–Zn ferrites. Ni–Zn ferrite powders with a nominal composition of  $\text{Ni}_{0.5}\text{Zn}_{0.5}\text{Fe}_2\text{O}_4$  were prepared from an exothermic reaction of a mixture of metallic nitrates (Ni, Zn and Fe), using urea as fuel. The materials used were zinc nitrate  $\text{Zn}(\text{NO}_3)_2 \cdot 6\text{H}_2\text{O}$  (Carlo Erba), nickel nitrate  $\text{Ni}(\text{NO}_3)_2 \cdot 6\text{H}_2\text{O}$  (Vetec), iron nitrate  $\text{Fe}(\text{NO}_3)_3 \cdot 9\text{H}_2\text{O}$  (Vetec) and urea ( $\text{NH}_2\text{CONH}_2$ ) (Synth). The proportions of the initial reagents were calculated based on the total valences of the reacting elements in order to supply the ratio [oxidizer (N)/fuel (U)]=1 to release the maximum energy for the reaction. The large quantity of gas that developed inhibited particle aggregation and yielded soft powders suitable for dispersion and use. The as-prepared combustion products, helium pycnometer and BET, which were characterized by XRD, showed a high specific surface area (44.26  $\text{m}^2/\text{g}$ ) and a very small particle and crystalline phase with atomic level homogeneity. The samples were uniaxially compacted by dry pressing and sintered at 1100°C, 1200°C, 1300°C and 1400°C for 2 h. The samples were characterized by bulk density, SEM, and B - H loop measurements. Optimum properties were obtained for samples sintered at 1200°C. The Ni–Zn ferrite presented a uniform microstructure with small grain size (2.0  $\mu\text{m}$ ), high density (95% TD) and significant hysteresis parameter values. The powder XRD patterns of  $\text{Ni}_{0.5}\text{Zn}_{0.5}\text{Fe}_2\text{O}_4$  prepared by combustion reaction showed a single-phase cubic spinel structure. The TEM results revealed that the particles sizes were not narrowly distributed. Thus, it can be inferred that the nucleation occurred as a single event, resulting in a size distribution of nuclei. The particle size calculated by TEM micrography was in the range of 11–30 nm.

G.S. Shahane et al.<sup>18</sup> synthesized nanocrystalline  $\text{Ni}_x\text{Zn}_{1-x}\text{Fe}_2\text{O}_4$  particles with compositions ( $x=0.1, 0.3, 0.5$ ) have been synthesized by a chemical co-precipitation method. The samples were characterized by X-ray diffraction, Fourier transform infrared spectroscopy, electron paramagnetic resonance, dc magnetization and ac susceptibility measurements. The X-ray diffraction patterns confirm the synthesis of single crystalline  $\text{Ni}_x\text{Zn}_{1-x}\text{Fe}_2\text{O}_4$  nanoparticles. The lattice parameter decreases with increase in Ni content resulting in a reduction in lattice strain. The Fourier transform infrared (FTIR) spectra of as-deposited samples were recorded with a NICOLET 5700 FTIR spectrometer in the range 4000–400  $\text{cm}^{-1}$ . The EPR measurements were carried out by a Varian E Line Century X-band EPR spectrometer (Model-E-112). The measurements were done at 9.36 GHz with modulation frequency 100 kHz. The lattice parameter decreases with increase in Ni content resulting in a reduction in lattice strain.<sup>35</sup> Similarly, crystallite size increases with the concentration of Ni. The magnetic measurements show the super paramagnetic nature of the samples for  $x=0.1$  and 0.3 whereas for  $x=0.5$  the material is ferromagnetic. The saturation magnetization is 23.95 emu/g and increases with increase in Ni content. The super paramagnetic nature of the samples is supported by the EPR and ac susceptibility measurement studies. N.D. Chaudhari et al.<sup>19</sup> synthesized Nickel zinc ferrites with generic formula,  $\text{Ni}_x\text{Zn}_{1-x}\text{Fe}_2\text{O}_4$  (with  $x=0.28\text{--}0.40$ ) by an oxalate precursor route starting with acetates to study their magnetic properties. Philips Diffractometer PW 1710 with  $\text{CuK}\alpha$  radiation was used for recording X-ray diffractograms. The XRD patterns indicate

that all the compositions exhibit single phase spinel structure. Microstructure of fractured surface of ferrite toroid was observed using scanning electron microscope (Cambridge Stereoscan-250 MKII)<sup>80</sup>. The system shows the presence of Yafet–Kittel type of spin. It is observed that magnetic moment (nB) values increase with the addition of Ni<sup>2+</sup>. The remanance ratio R tends to increase with the addition of Ni<sup>2+</sup>, which has been attributed to the increase of magnetocrystalline anisotropy constant (K1). The values of R compare well with the theoretical value (0.87). The coercive force decreases with the addition of Ni<sup>2+</sup> concentration whereas the value of remanance ratio increases with the addition of Ni<sup>2+</sup>. Studies on temperature variation of R and Hc reveal that these parameters are thermally insensitive, which confirms the presence of multi domain grains in the material.

Sanjeev Kumar et al.<sup>20</sup> carried out synthesis of monodisperse Ni, Zn-ferrite (Ni<sub>1-x</sub>Zn<sub>x</sub>Fe<sub>2</sub>O<sub>4</sub>, x<sup>1</sup>/<sub>4</sub>1, 0.8, 0.6, 0.5, 0.4, 0.2, 0.0) nano-crystals has been achieved by the inverse microemulsion method using CTAB as surfactant and kerosene as an oil phase. The detailed characterization of the synthesized nanocrystals and measurement of the magnetic properties has been done by techniques like X-ray diffraction (XRD), field emission transmission electron microscopy (FETEM), Fourier transform infrared spectroscopy (FITR) and Vibrating Sample Magnetometer (VSM) respectively. The Debye–Scherrer equation has been used to calculate the crystallite size of the ferrite nanocrystals from the broadening of the XRD peak intensity after K $\alpha$ 2 corrections. Prior to taking measurement, the dispersed Nano crystals in water were placed on carbon coated 400 mesh copper grids and were allowed to dry at room temperature. Lakeshore 7304 Vibrating Sample Magnetometer (VSM) was used to record the hysteresis loops of the powder samples at various temperatures. The relationship between the structure and composition of the nanocrystals with magnetic properties has been investigated. The nanocrystals size is found to be in the range 1–5 nm<sup>78</sup>. The effect of Zn substitution on size and magnetic properties has been studied. It has been observed that magnetism changed from ferromagnetic at X<sup>1</sup>/<sub>4</sub> 0 to super paramagnetic to paramagnetic at X<sup>1</sup>/<sub>4</sub>1 as Zn concentration increased. The Curie temperature is found to decrease with an increase in Zn concentration.

A.S. Džunuzović et al.<sup>21</sup> synthesized the nanoparticles of Ni<sub>1-x</sub>Zn<sub>x</sub>Fe<sub>2</sub>O<sub>4</sub> (x<sup>1</sup>/<sub>4</sub>0.0, 0.3, 0.5, 0.7, 1.0, denoted as NF, NZF (70–30), NZF (50–50), NZF (30–70) and ZF) by the auto-combustion method. The phase and crystal structure analysis was carried out by an X-ray diffraction technique (Model Phillips PW1710 diffractometer, Co K $\alpha$  radiation, 0.51/min). The average crystallite size was calculated by Debye–Scherrer's equation using data obtained from X-ray diffractograms. Raman spectra were collected in the backscattering micro-Raman configuration using a Jobin Yvon T64000 spectrometer equipped with a nitrogen-cooled CCD detector. The measurements were performed at room temperature. The morphology and microstructure of obtained powders and ceramics were examined using a scanning electron microscope (SEM Model TESCAN SM-300). Magnetic measurements of materials were carried out using a superconducting quantum interferometric magnetometer SQUID (Quantum Design). X-ray analysis indicated the formation of well crystallized Ni–Zn ferrite phases, and Raman spectroscopy enabled a precise phases identification. The change of the grain size and density with increasing Zn content was confirmed by scanning electron microscopy.

Magnetization of saturation and remnant magnetization, both, continuously increase up to  $x \leq 0.3$  of Zn, and then decrease for more Zn. The influence of the grain size of investigated systems on the saturation magnetization was studied. Impedance spectroscopy measurements were carried out in order to investigate the electrical resistivity of materials, showing that grain boundaries have greater impact on total resistivity than grains. J. Gutiérrez-López et al.<sup>22</sup> synthesized Ni–Zn ferrites by Powder Injection Moulding (PIM). Two different manufacturing ways were used: powder injection moulding and uniaxial compaction. In the case of PIM, powder-binder mixtures were prepared by a twin-screw extruder Thermohaake Rheomex CTW100p with a temperature profile of 160–165–170 °C and a screw speed of 40 rpm. They analyzed the sintering process, between 900 °C and 1300 °C, of Ni–Zn ferrites prepared by PIM. In particular, the densification behaviour, microstructure and mechanical properties of samples with toroidal and bar geometry were analyzed at different temperatures. Additionally, the magnetic behaviour (complex permeability and magnetic losses factor) of these compacts was compared with that of samples prepared by conventional powder compaction. Finally, the mechanical behaviour (elastic modulus, flexure strength and fracture toughness) was analyzed as a function of the powder loading of feedstock. The final microstructure of prepared samples was correlated with the macroscopic behaviour. A good agreement was established between the densities and population of defects found in the materials depending on the sintering conditions. In general, the final mechanical and magnetic properties of PIM samples were enhanced relative to those obtained by uniaxial compaction.

S. S. Kumbhar et al.<sup>23</sup> synthesized thin films of nickel-zinc ferrite with general formula  $\text{Ni}_x\text{Zn}_{1-x}\text{Fe}_2\text{O}_4$  (where  $x = 0.5, 0.6, 0.7, 0.8, 0.9, 1.0$ ) using spray pyrolysis technique onto the glass substrates at optimized substrate temperature of 400 °C. The nickel nitrate, zinc acetate and ferric nitrate were used as precursor materials with double distilled water as solvent. As deposited films are annealed at 600 °C for 2 hrs. The soda-lime glass substrates were used for film deposition<sup>65</sup>. The X-ray diffraction (XRD) analysis reveals that the  $\text{Ni}_x\text{Zn}_{1-x}\text{Fe}_2\text{O}_4$  thin films are polycrystalline with spinel cubic structure. The SEM images show the films are smooth and uniform in nature. To understand the semiconducting behavior the DC resistivity of films was measured using two-point probe method. To know the conduction mechanism of ferrites the AC conductivity of thin films was measured. The linear nature of the graph shows the small type of polarons. Frequency dependence of dielectric constant shows dielectric dispersion due to the Maxwell-Wagner type of interfacial polarization. Impedance spectroscopy used to study electrical behavior of grain or grain boundaries. It is seen that as the nickel content increases the crystallite size varies from 20 to 36 nm.

Wei Yan et al.<sup>24</sup> synthesized monodisperse Ni–Zn ferrites ( $\text{Ni}_x\text{Zn}_{1-x}\text{Fe}_2\text{O}_4$ ) microspheres by solvothermal method. X-ray diffraction pattern (XRD), transmission electron microscope (TEM), field emission scanning electron microscopy (FE-SEM) and vibrating sample magnetometry are used to characterize the shape, structure, size and magnetic properties of the as-synthesized magnetic microspheres. The crystallinity and structure of the  $\text{Ni}_x\text{Zn}_{1-x}\text{Fe}_2\text{O}_4$  microspheres at the reaction temperature 200 °C and the reaction time 12 h were confirmed by powder X-ray diffraction. The powder XRD patterns revealed the formation of the single-phase

spinel structure for the synthesized materials. TEM and FE-SEM show the size and morphology of the as-synthesized sample in detail. The maximum magnetic saturation value of the  $\text{Ni}_{0.2}\text{Zn}_{0.8}\text{Fe}_2\text{O}_4$  microspheres can reach  $60.6 \text{ emu g}^{-1}$ . These magnetic  $\text{Ni}_x\text{Zn}_{1-x}\text{Fe}_2\text{O}_4$  microspheres are expected to have wide applications in bio-nanoscience and electronic devices technology.

Deng Ni et al.<sup>25</sup> synthesized Nickel-zinc ferrites (Ni-Zn ferrites) nanocomposites by a solvothermal method and characterized by X-ray diffraction (XRD), scanning electronic microscope (SEM) and vibrating sample magnetometer (VSM). The effects of solvothermal parameters such as ratio of  $\text{Ni}^{2+}$  to  $\text{Zn}^{2+}$ , the temperature and the time of solvothermal reaction on the magnetic properties and the microstructures of Ni-Zn ferrites were investigated. Results demonstrate that with raising of reaction time, the particles become bigger and more homogeneous, and the saturation magnetization of the Ni-Zn ferrites nanocomposites get higher; and the formation temperature of Ni-Zn ferrites spherical particles is  $180 \text{ }^\circ\text{C}$ ; raising  $\text{Ni}^{2+}$  concentration in the Ni-Zn ferrites could not change their morphologies. The saturation magnetization of the Ni-Zn ferrites increases with the increase of  $\text{Ni}^{2+}$  in the product; it will reach the highest when  $\text{Ni}^{2+}$  concentration is up to  $x=0.30$  while it will be the lowest when  $\text{Ni}^{2+}$  concentration is down to  $x=0.20$ . H.Y. Luo et al.<sup>26</sup> synthesized  $\text{Ni}_{0.5}\text{Zn}_{0.5}\text{Fe}_2\text{O}_4$  – forsterite composites by a sol-gel method. X-ray diffraction and SEM were used to characterize the crystallization behavior of the composite samples which were heat treated at temperatures varying from  $800$  to  $1100 \text{ }^\circ\text{C}$ . The results showed that  $\text{Ni}_{0.5}\text{Zn}_{0.5}\text{Fe}_2\text{O}_4$  and forsterite ( $\text{Mg}_2\text{SiO}_4$ ) can co-crystallize and the crystallites grow even more larger with increasing heat-treatment temperature. High-frequency ( $10 \text{ MHz} - 1 \text{ GHz}$ ) magnetic and dielectric properties of the composite samples were presented. Permeability increased with heat-treatment temperature. Quality factor was found to be two orders higher than that of equivalent pure, bulk ferrite.

N. Rezlescu et al.<sup>27</sup> investigated the effects of four additives ( $\text{Sb}_2\text{O}_3$ ,  $\text{Na}_2\text{O}$ ,  $\text{CaO}$  and  $\text{ZrO}_2$ ) on the properties of  $\text{Ni}_{0.255}\text{Zn}_{0.745}\text{Fe}_2\text{O}_4$  ferrite, having Curie point around  $0^\circ\text{C}$ .  $\text{Na}_2\text{O}$  and  $\text{Sb}_2\text{O}_3$  favour the densification of the ferrite at low temperature, but increase  $T_c$ .  $\text{CaO}$  improves the density and decreases  $T_c$ . All additives improve the temperature dependence of  $\mu_i$  and the electrical resistivity. The best additive seems to be  $\text{CaO}$  which accomplishes the best compromise with respect to the density, electrical resistivity and the shape of  $\mu_i - T$  curve. Yong Choi et al.<sup>24</sup> synthesized the  $\text{Ni}_x\text{Zn}_{1-x}\text{Fe}_2\text{O}_4$  ferrites by self-propagating high-temperature synthesis at the oxygen partial pressures of  $0.5$  and  $5.0 \text{ MPa}$ . Neutron diffraction revealed that the final stoichiometries of the ferrites were  $\text{Ni}_{0.38}\text{Zn}_{0.62}\text{Fe}_2\text{O}_4$  and  $\text{Ni}_{0.33}\text{Zn}_{0.67}\text{Fe}_2\text{O}_4$ , respectively. As the oxygen pressure changed from  $0.5$  to  $5.0 \text{ MPa}$ , the coercive force ( $H_c$ ) and residual magnetization ( $M_r$ ) decreased about  $55$  and  $30\%$ , respectively. Whereas, the maximum magnetization ( $M_s$ ), susceptibility ( $\Delta M/\Delta H$ ) and curie temperature increased about  $14$ ,  $65$  and  $2.5\%$ , respectively. The improved magnetic properties are attributed to the increased spinel formation due to oxygen pressure during the self-propagating high temperature synthesis and different non-stoichiometric numbers of the ferrites due to the competitive reduction reaction between nickel oxide and zinc oxide.

H. Gul et al.<sup>28</sup> synthesized Nickel zinc ferrite nanoparticles  $\text{Ni}_{1-x}\text{Zn}_x\text{Fe}_2\text{O}_4$  ( $x = 0.25, 0.5, 0.75, 1$ ) by the chemical co-precipitation route. The samples were characterized by X-ray diffraction

(XRD), DC electrical resistivity, dielectric constant and low field AC magnetic susceptibility. The powder XRD patterns confirm the single phase spinel structure for the synthesized materials. The crystallite size was calculated from the most intense peak (3 1 1) using the Scherrer formula. The crystallite size was found within the range 7–15 nm. The crystallite size decreases with increasing zinc concentration. DC electrical resistivity decreases as the temperature increases indicating that the samples have semiconductor like behavior. DC electrical resistivity of the samples at room temperature was found to vary from  $1.67 \times 10^9$  to  $4 \times 10^9 \Omega \text{ cm}$  with zinc concentration. The activation energy and drift mobility were calculated from DC electrical resistivity measurements. The dielectric constant for all the compositions has been studied as a function of frequency in the range from 500 Hz to 1MHz at room temperature. The dielectric constant follows the Maxwell–Wagner interfacial polarization. AC magnetic susceptibility measurements were carried out as a function of temperature to measure the transition temperature, which was found to decrease with zinc concentration.

Yutaka Shimada et al.<sup>29</sup> investigated Initial permeability of Ni–Zn ferrite films prepared by spin spray chemical plating. They exhibit a semi–hard magnetization process but have relatively high permeability with explicit dual peak resonance loss in the GHz frequency range. In this study, it turned out that the loss is determined mainly by the two magnetic parameters, namely, the crystalline anisotropy and a uniaxial anisotropy induced by Co addition. Measurement of permeability in an external DC field clarified that the semi-hard wall coercivity fixes the spin direction of residual magnetization state and, consequently, gives rise to uniaxial permeability with dependence of its direction on the previously applied DC field. S. Zahi<sup>30</sup> synthesized the Ni–Zn ferrite powder, with a composition of  $\text{Ni}_{0.25}\text{Zn}_{0.75}\text{Fe}_2\text{O}_4$  and fabricated by sol–gel method at low and high temperatures. The prepared low and high-temperature sintered N–Zn ferrite of free defects could possess excellent electromagnetic properties, as well as fine-grained microstructures, for electronic applications with high performance and low cost. The results gathered from the X-ray diffraction (XRD) indicated the amount of single-phase spinel ferrite constituents could be formed at a temperature below 400 °C. The Fourier transform-infrared spectroscopic (FT-IR) and the analyses using the microscopic photomicrographs were used to identify the formation of Ni–Zn spinel ferrite. The initial magnetic permeability showed that the inductance of the fabricated ferrite cores was of the highest value. Therefore, a laboratory coil equipped with a high-temperature superconducting magnetic energy storage (HT-SMES) was designed. The theoretical analysis of the torus with rectangular shaped coils was also carried out, and for this, a consideration for the average magnetic field inside the torus was used to calculate the inductance of the shape. Using uninterruptible power supply (UPS) and power conditioning system (PCS) which give details of the application of I-SMES in solving voltage sag, a schematic diagram is also reported.

S. S. Kumbhar et al.<sup>23</sup> synthesized Thin films of nickel-zinc ferrite with general formula  $\text{Ni}_x\text{Zn}_{1-x}\text{Fe}_2\text{O}_4$  (where  $x = 0.5, 0.6, 0.7, 0.8, 0.9, 1.0$ ) by spray pyrolysis technique onto the glass substrates at optimized substrate temperature of 400 °C. The nickel nitrate, zinc acetate and ferric nitrate were used as precursor materials with double distilled water as solvent. As deposited films are annealed at 600 °C for 2 hrs. The X-ray diffraction (XRD) analysis reveals

that the  $\text{Ni}_x\text{Zn}_{1-x}\text{Fe}_2\text{O}_4$  thin films are polycrystalline with spinel cubic structure. The SEM images shows the films are smooth and uniform in nature. To understand the semiconducting behavior the DC resistivity of films was measured using two point probe method. To know the conduction mechanism of ferrites the AC conductivity of thin films was measured. The linear nature of the graph shows the small type of polarons. Frequency dependence of dielectric constant shows dielectric dispersion due to the Maxwell-Wagner type of interfacial polarization. Impedance spectroscopy used to study electrical behavior of grain or grain boundaries.

J. Jadhav et al.<sup>31</sup> synthesized Nanocrystalline Ni-Zn ferrites ( $\text{Ni}_x\text{Zn}_{1-x}\text{Fe}_2\text{O}_4$ ,  $x = 0.2-0.8$ ) by a novel and facile chemical method via a polymer precursor and their structural and magnetic properties were evaluated and discussed in correlation with the cationic distribution. The synthesis process involves a reaction of aqueous solutions of metal ( $\text{Fe}^{3+}$ ,  $\text{Zn}^{2+}$  and  $\text{Ni}^{2+}$ ) salts with an aqueous polyvinyl alcohol (PVA)-sucrose solution at 60-65°C. Controlled growth of the ferrite nanoparticles in terms of both composition and morphology was achieved by encapsulation of the nucleating sites in the PVA-sucrose polymer micelles. All the derived samples show single phase of cubic spinel structure (Fd3m space group). The microstructural features in the derived samples were evaluated with a field emission scanning electron microscope (FESEM) and a high-resolution transmission electron microscope (HRTEM). Structural properties of the derived samples were studied with X-ray diffraction (XRD), X-ray absorption near edge structure (XANES), extended X-ray absorption fine structure (EXAFS), Raman spectroscopy, energy dispersive X-ray (EDX) analysis, and Fourier transformed infrared (FTIR) spectroscopy. Magnetic properties of the derived samples were studied with a vibrating sample magnetometer (VSM) at room temperature. The distribution of cations at the lattice sites has significant influence on the magnetic properties of the ferrite samples. The magnetization increases with the increase in Ni concentration in the samples till the maximum magnetization is observed in the composition  $\text{Ni}_{0.5}\text{Zn}_{0.5}\text{Fe}_2\text{O}_4$ . Further increase in Ni concentration reduces the magnetization. The results were explained on the basis of inter sub-lattice and intra sub-lattice coupling interactions between cations in A and B-sites.

Jeevan Job Thomas et al.<sup>31</sup> synthesized  $\text{Ni}_{0.5}\text{Zn}_{0.5}\text{Fe}_2\text{O}_4$  nanoparticles through sol-gel synthesis method using poly vinyl alcohol (PVA) as the chelating agent. Sintering at elevated temperatures was employed to obtain samples with higher particle sizes. It is found that even though the particle size changes with the increase in sintering temperature there is no obvious change in the relative population of the octahedral and tetrahedral sites for the samples in the present study. The structural characterization using X-ray diffraction suggests that the three samples possess uniform cation distribution. The variation of magnetization as a function of applied magnetic field at room temperature is studied using a vibrating sample magnetometer and all the samples found to exhibit nearly zero remanence and zero coercivity suggesting a superparamagnetic behaviour. The variation of magnetizations of the three different samples with temperature was studied by ZFC-FC technique at two different applied fields of 10 Oe and 1000 Oe. In order to study the possibility of structural changes, chemical and coordination differences of iron in the nanocrystalline Ni-Zn ferrite particles, room temperature  $^{57}\text{Fe}$  Mössbauer spectroscopy study was used. The application of 5 T magnetic field at 5 K

temperature resolves the two sub spectra and canting angle of  $27^\circ$  and  $12^\circ$  were observed which clearly indicates the noncollinear magnetic alignment in nano crystallites of  $\text{Ni}_{0.5}\text{Zn}_{0.5}\text{Fe}_2\text{O}_4$ . The neutron diffraction study was performed at seven different temperatures 20, 50, 100, 150, 200, 250 and 300 K. Rietveld refinement of the neutron diffraction data was performed to deduce the basic structural parameters, cation distribution and micro level magnetic alignments in the nanosized nickel zinc ferrite

Wei Yan et al.<sup>26</sup> synthesized Monodisperse Ni–Zn ferrites ( $\text{Ni}_x\text{Zn}_{1-x}\text{Fe}_2\text{O}_4$ ) microspheres via solvothermal method. X-ray diffraction pattern (XRD), transmission electron microscope (TEM), field emission scanning electron microscopy (FE-SEM) and vibrating sample magnetometry are used to characterize the shape, structure, size and magnetic properties of the as-synthesized magnetic microspheres. The powder XRD patterns revealed the formation of the single-phase spinel structure for the synthesized materials. TEM and FE-SEM show the size and morphology of the as-synthesized sample in detail. The maximum magnetic saturation value of the  $\text{Ni}_{0.2}\text{Zn}_{0.8}\text{Fe}_2\text{O}_4$  microspheres can reach  $60.6 \text{ emu g}^{-1}$ . These magnetic  $\text{Ni}_x\text{Zn}_{1-x}\text{Fe}_2\text{O}_4$  microspheres are expected to have wide applications in bionanoscience and electronic devices technology. Intan Helina Hasan et al.<sup>32</sup> studied and investigated the properties of nickel zinc ferrite ( $\text{Ni}_{0.5}\text{Zn}_{0.5}\text{Fe}_2\text{O}_4$ ) thick film with  $\text{Ni}_{0.5}\text{Zn}_{0.5}\text{Fe}_2\text{O}_4$  nanopowders as active powders and linseed oil as the organic vehicle.  $\text{Ni}_{0.5}\text{Zn}_{0.5}\text{Fe}_2\text{O}_4$  thick film paste samples have been prepared with various weight ratios to study the rheology properties of the pastes. Rheology results show that paste with 30% wt.  $\text{Ni}_{0.5}\text{Zn}_{0.5}\text{Fe}_2\text{O}_4$  has suitable rheological shear-thinning behavior, which is required for formulating screen printing pastes. Morphology studies show that at a low firing temperature of  $200^\circ\text{C}$ , the thick film exhibits good adhesion to the substrate as well as excellent removal of the organic vehicle, due to the use of linseed oil which is well known as a fast-drying oil in the painting industry. The dielectric and magnetic properties of the thick film with linseed oil as the organic vehicle show good results comparable to the work being done in ferrite thick film research groups. The inclusion of  $\text{Ni}_{0.5}\text{Zn}_{0.5}\text{Fe}_2\text{O}_4$  thick film in the fabrication of microstrip patch antenna resulted in improved return loss by 64.22%, and in bandwidth by 84.61% increase, proving that the ferrite thick film can significantly enhance the performance of the antenna, as well as opening up many possibilities in the application for microwave device.

K.Kondo et al.<sup>33</sup> investigated Polycrystalline  $\text{Ni}_{0.34}\text{Cu}_{0.12}\text{Zn}_{0.56}\text{Fe}_{1.98}\text{O}_4$  with different grain sizes up to 39 nm. At the frequency of 50 kHz, both the hysteresis loss under the excitation condition of 150 mT and the initial permeability decreased with increasing grain size. These results were interpreted in terms of the contribution of grain boundaries and pores inside the grains to the domain wall pinning. F.S. Li et al.<sup>34</sup> synthesized  $\text{Ni}_{1-x}\text{Zn}_x\text{Fe}_2\text{O}_4$  ( $0.0 \leq x \leq 1.0$ ) nanoparticles by the polyvinyl alcohol (PVA) sol-gel method. The lattice parameter of Ni-Zn nanoparticle is larger than that of the bulk material. The crystalline structure has been investigated by X-ray diffraction (XRD). The Mossbauer spectra of the samples showed the presence of ultrafine particles exhibiting super paramagnetic relaxation at room temperature and an ordered magnetic structure at 77 K.

Antoinette MORELL synthesized Submicronic Ni-Zn ferrite powder by the coprecipitation technology was sintered by hot-pressing, conventional and fast-firing. Sintering conditions were determined. The powder, compacted by isostatic or axial pressing, was sintered according to three different types of sintering: hot-pressing, conventional and fast-sintering. In all cases, permeabilities higher than 1500 were obtained. Microstructures of the ceramics revealed that the grains are small (less than 10  $\mu\text{m}$ ). By combining sintering temperatures and overall cycle times, it is possible to achieve sintered materials with high magnetic permeability. Neha Aggarwal et al.<sup>35</sup> synthesized Nickel zinc ferrites,  $\text{Ni}_{1-x}\text{Zn}_x\text{Fe}_2\text{O}_4$  ( $x=0.0, 0.2, 0.4, 0.6, 0.8$  and  $1.0$ ) using sol-gel citrate precursor route. Sintering of the ferrite powder was done at  $1000^\circ\text{C}$  for 8 h in high temperature muffle furnace. Vibrating Sample Magnetometer (VSM) has been employed to determine the magnetic properties. The electromagnetic and absorption properties have been determined using Vector Network Analyzer (VNA) in Ku band (12.4-18 GHz). RL as low as -31.17 dB (~99.92% absorption) has been obtained for composition  $x=0.2$  at a pellet thickness of 3 mm. Such a low value of RL makes these Nickel-Zinc ferrites excellent absorbers, which can work at gigahertz frequencies in different applications such as radar stealth technology. Seung Wha Lee et al.<sup>36</sup> synthesized Nanoparticles  $\text{Ni}_{0.7}\text{Zn}_{0.3}\text{Fe}_2\text{O}_4$  were synthesized by a sol-gel method.  $\text{Ni}_{0.7}\text{Zn}_{0.3}\text{Fe}_2\text{O}_4$  powders annealed at  $300^\circ\text{C}$  compose a spinel structure and behaved super paramagnetically, while annealed at 400 and  $500^\circ\text{C}$  have typical spinel structure with ferrimagnetism in nature. The mean size of  $\text{Ni}_{0.7}\text{Zn}_{0.3}\text{Fe}_2\text{O}_4$  nanoparticle is about 11 nm. The hyperfine fields at 13 K for the tetrahedral (A) and the octahedral (B) patterns were found to be 499 and 523 kOe, respectively. Blocking temperature ( $T_B$ ) of  $\text{Ni}_{0.7}\text{Zn}_{0.3}\text{Fe}_2\text{O}_4$  nanoparticle is about 260 K. Also, temperature increased up to 43  $^\circ\text{C}$  within 7 min under AC magnetic field of 7MHz. It is considered that 11 nm sample is available for biomedical applications such as hyperthermia and drug delivery system as a magnetic fluid carrier because it has spherical shape, narrow particle distribution, chemical stability, and SPM behavior.

Yutaka Shimada et al.<sup>29</sup> investigated Initial permeability of Ni-Zn ferrite films prepared by spin spray chemical plating. They exhibit a semi hard magnetization process but have relatively high permeability with explicit dual peak resonance loss in the GHz frequency range. In this study, it turned out that the loss is determined mainly by the two magnetic parameters, namely, the crystalline anisotropy and a uniaxial anisotropy induced by Co addition. Measurement of permeability in an external DC field clarified that the semi-hard wall coercivity fixes the spin direction of residual magnetization state and, consequently, gives rise to uniaxial permeability with dependence of its direction on the previously applied DC field.

Souilah Zahi et al.<sup>37</sup> synthesized , the Ni-Zn ferrite powder of a  $\text{Ni}_{0.3}\text{Zn}_{0.7}\text{Fe}_2\text{O}_4$  composition by sol-gel route using metal acetates at low temperatures. Both the scanning electron microscope and X-ray diffraction analyses of various gel samples heated at different temperatures were used to identify the reaction stages where the amorphous-gel-to-crystalline phase transition occurred. The electrical, magnetic and microstructural properties of the toroidal cores were studied. It was found that the initial permeability increased with a large frequency band (0.1-31.39 MHz) and the magnetic loss was small. The electrical resistivity

was higher as compared to the ones which were obtained by the conventional process. Therefore, well-defined polycrystalline microstructure nickel-zinc ferrite and a short processing time of gel preparation have become the major achievements of this study.

I.H. Gul et al.<sup>28</sup> synthesized Nickel zinc ferrite nanoparticles  $\text{Ni}_{1-x}\text{Zn}_x\text{Fe}_2\text{O}_4$  ( $x = 0.25, 0.5, 0.75, 1$ ) by the chemical co-precipitation route. The samples were characterized by X-ray diffraction (XRD), DC electrical resistivity, dielectric constant and low field AC magnetic susceptibility. The powder XRD patterns confirm the single phase spinel structure for the synthesized materials. The crystallite size was calculated from the most intense peak (3 1 1) using the Scherrer formula. The crystallite size was found within the range 7–15 nm. The crystallite size decreases with increasing zinc concentration. DC electrical resistivity decreases as the temperature increases indicating that the samples have semiconductor like behavior. DC electrical resistivity of the samples at room temperature was found to vary from  $1.67 \times 10^9$  to  $4 \times 10^9 \Omega \text{ cm}$  with zinc concentration. The activation energy and drift mobility were calculated from DC electrical resistivity measurements. The dielectric constant for all the compositions has been studied as a function of frequency in the range from 500 Hz to 1MHz at room temperature. The dielectric constant follows the Maxwell–Wagner interfacial polarization. AC magnetic susceptibility measurements were carried out as a function of temperature to measure the transition temperature, which was found to decrease with zinc concentration. . It has been observed that drift mobility increases by increasing temperature.

Rau 1 Valenzuela et al.<sup>38</sup> synthesized Ferrite nanoparticles of composition  $\text{Zn}_{0.5}\text{Ni}_{0.5}\text{Fe}_2\text{O}_4$  were by forced hydrolysis in polyol from the corresponding zinc, nickel and iron acetates. By varying the preparation conditions, different aggregation states were obtained, ranging from isolated nanoparticles with average diameter of 5 nm, to clusters of some 20 nm, formed as well by nanoparticles with average diameter in the 5 nm range, as confirmed by X-ray diffraction and high-resolution transmission electron microscopy. Ferromagnetic resonance measurements exhibited a ferrimagnetic behavior for both aggregation states at 77 K; at 300 K, however, isolated nanoparticles showed a superparamagnetic behavior while clustered ones remained ferrimagnetic with a broad linewidth. These results are interpreted on the basis of interactions between nanoparticles. Finally, an explanation based on the differences between measuring time and relaxation time was proposed to account for the differences observed in the blocking temperature, as determined by ZFC–FC and FMR measurements.

M.U. Islam et al.<sup>39</sup> synthesized fine particles Ni–Zn ferrites by Co-precipitation technique using chlorides of constituents. The particle size was estimated from X-ray diffraction data using Sherrer’s formula. The dc electrical resistivity and thermo-power was measured in the temperature range 300–450 K and it was found that all the samples are degenerate type semi-conductors. The results of dc resistivity and thermo-electric power confirm that the conduction mechanism in these ferrites is due to small polaron hopping. R.V. Mangalaraja et al.<sup>40</sup> synthesized Ni-Zn ferrite of composition  $\text{Ni}_{0.8}\text{Zn}_{0.2}\text{Fe}_2\text{O}_4$  prepared by the non-conventional flash combustion technique and the initial permeability ( $\mu_i$ ) and relative loss factor ( $\tan \delta/\mu_i$ ) of it are studied and reported. The ferrite powder prepared by this technique was calcined at

900 °C and the uniaxially pressed samples were sintered at various temperatures 1150, 1250 and 1350 °C. The initial permeability and the relative loss factor have been studied as the function of testing frequency and temperature. It is observed that the Ni-Zn ferrites prepared by this technique have the initial permeability from 16 to 20 in the frequency range 1 kHz to 13 MHz and the relative loss factor of  $10^3 - 10^4$  in the frequency range 100 kHz to 13 MHz. The initial permeability increases from room temperature to 300 °C. The relative loss factor is of the order of  $10^{-2}$ . The results obtained are better when compared with ferrites prepared by the conventional ceramic method. This is attributed to better purity, controlled microstructure and chemical homogeneity achievable by the flash combustion method. Low relative loss factor makes these ferrites particularly useful as inductor and transformer materials for high frequency applications. The ferrite materials prepared by this technique are pure, highly reactive because of the atomic level mixing of the starting materials. The ferrites by this technique are having better microstructure and high chemical homogeneity, which result in good magnetic properties.

Yong Choi et al.<sup>41</sup> synthesized the  $Ni_x Zn_{x-1}Fe_2O_4$  ferrites by self-propagating high-temperature synthesis at the oxygen partial pressures of 0.5 and 5.0 MPa. Neutron diffraction revealed that the final stoichiometries of the ferrites were  $Ni_{0.38}Zn_{0.62}Fe_2O_4$  and  $Ni_{0.33}Zn_{0.67}Fe_2O_4$ , respectively. As the oxygen pressure changed from 0.5 to 5.0 MPa, the coercive force ( $H_c$ ) and residual magnetization ( $M_r$ ) decreased about 55 and 30%, respectively. Whereas, the maximum magnetization ( $M_s$ ), susceptibility ( $\Delta M/\Delta H$ ) and curie temperature increased about 14, 65 and 2.5%, respectively. The improved magnetic properties is attributed to the increased spinel formation due to oxygen pressure during the self-propagating high temperature synthesis and different non-stoichiometric numbers of the ferrites due to the competitive reduction reaction between nickel oxide and zinc oxide. Purushotham Yadoji et al.<sup>42</sup> synthesized  $Ni_{1-x}Zn_xFe_2O_4$  with  $x= 0.0 - 1.0$  by conventional and microwave sintering procedures using high purity NiO, ZnO and  $Fe_3O_4$  in stoichiometric proportions. Pellets made out this powder have been sintered using both microwave and conventional procedures at 1275 °C for 30 min. Microstructural study revealed large, but fewer pores in the microwave sintered specimens and small, but substantially more pores in the case of conventionally sintered specimens. Magnetic properties measurements showed lower coercivity and higher magnetization values for microwave sintered specimens. Lower coercivity values observed in microwave sintered specimens are attributed to larger grain size and higher magnetization values may be explained by the contribution of the ‘microwave field’ to the ‘uncoupling spin effect’. Most significantly samples sintered in a microwave field, generally, showed lower dielectric constant values compared with the samples sintered conventionally, making microwave sintering particularly suitable for high frequency applications.

Sanjeev Kumar et al.<sup>20</sup>. Monodisperse Ni, Zn-ferrite ( $Ni_{1-x}Zn_xFe_2O_4$ ,  $x=1, 0.8, 0.6, 0.5, 0.4, 0.2, 0.0$ ) nanocrystals have been prepared by the inverse microemulsion technique using CTAB as surfactant and kerosene as an oil phase. Further, characterization of the synthesized nanocrystals and measurement of the magnetic properties has been done by techniques like X-ray diffraction (XRD), field emission transmission electron microscopy (FETEM), Fourier

transform infrared spectroscopy (FITR) and Vibrating Sample Magnetometer (VSM) respectively. The relationship between the structure and composition of the nanocrystals with magnetic properties has been investigated. The nanocrystallite size varies from 1 to 5 nm. Nanocrystals with different Ni and Zn compositions were obtained by changing the proportion of the reactants. It has been observed that magnetism changed from ferromagnetic at  $X=0$  to super paramagnetic to paramagnetic at  $X=1$  as Zn concentration increased. The Curie temperature is found to decrease with an increase in Zn concentration.

The size of the nanocrystals increases as the Ni content decreases or vice versa. Intern the magnetic behavior changes from ferro-magnetic at  $x=0$  to superparamagnetic to paramagnetic at  $x=1$  as the Zn concentration increases. The smaller crystals exhibit an increased Curie temperature (TC) which can be ascribed to random cation distribution and unique finite size scaling. The Curie temperature decreases with Zn concentration. The decrease of Curie temperature with non-magnetic Zn concentration has been explained by the A–B exchange interaction strength due to the change of  $Fe^{3+}$  distribution between A and B sites. The mono-dispersed multicomponent ferrite nanocrystals could provide a novel perspective on the inter particle interactions between different cations ( $Ni^{2+}$ ,  $Zn^{2+}$ , or both), which play a major role in magnetic properties.

A. Safaria et al.  $Ni_{0.5}Zn_{0.5}Fe_2O_4$  powders were prepared by plasma arc discharge method followed by the subsequent heat treatments within the temperature range of 1000–1250 °C. Structural, microstructural, magnetic and dielectric properties of the as-synthesized and heat-treated powders were examined. The results indicate that as-synthesized powders contain a mixture of ZnO,  $Fe_{0.72}OZn_{0.13}$  and Ni-Zn ferrite phases. However, the quantitative amount of Ni-Zn ferrite phase gradually increases by post annealing process. This finding is accompanied by an improvement in the magnetic properties such that a single-phase Ni-Zn ferrite with the average crystallite size of 212 nm, lattice parameter of 8.332 Å, saturation magnetization of 35.1 emu/g and coercivity of 24.9 Oe is formed after annealing at 1250 °C. Nevertheless, dielectric properties measured in the frequency range 20 Hz–10 MHz exhibits a complex behaviour due to the different mechanisms that cause polarization.

Z. W. Li et al. studied for  $Ni_{0.97-x}Zn_xCo_{0.03}Fe_2O_4$  spinel ferrites with composition  $x=0.5$  and 0.65A. A mixture of NiO, ZnO,  $Co_3O_4$  and  $Fe_2O_3$  were taken in appropriate ratio for the nickel cobalt ferrite by solvothermal method. They used various techniques to study and characterise their samples like XRD, electron microscopy, Mossbauer spectroscopy. They reported that this material can be in future be used in spintronics, magneto-electronics and ultra-high-density recording media as well as radar absorbing applications. Among the soft magnetic materials NiZn ferrites have received special attention because of their good magnetic properties and high electric resistivity over a wide range of frequencies but they did show low permeability. Similarly, MnZn showed high permeabilities and high magnetisation but showed low resistivity and high eddy currents losses. Co ferrites also showed high permittivity values therefore researchers are working on combination of these ferrites like Ni-Mn-Zn and Ni-Co-Zn ferrites.

J. Kulikowski et al. prepared Co substituted Ni-Zn ferrite and studied the effect of small cobalt content on magnetostriction of Ni-Zn ferrites. X. Shen et al. prepared Ni-Zn-Co ferrite granular films of 1.5 micrometers in thickness and prepared on glass substrates by the spray plating method at 90° C. The produced films were characterised using a field emission scanning electron microscope and hysteresis loops measurements via a vibrating sample magnetometer. The film exhibited large formation of spinel ferrites and were calcined at 1080° C for 4 hours. The calcined samples were then crushed and ball-milled and finally, the powder was shaped and sintered at 1200 -1300° C for 4 hours. The spinel ferrites exhibited excellent EM attenuation characteristics with low refractivity and broad bandwidth free at very high frequency at ultra-high frequency bands. The permittivity was found to increase as the sintering temperature was increased.

S. Heini et al. have studied the microstructural, magnetic and electric properties of  $Zn_{0.4}Ni_{0.3}Co_{0.3}Fe_2O_4$  (ZNCFO) and  $Zn_{0.4}Cu_{0.3}Co_{0.3}Fe_2O_4$  (ZCCFO) ferrites were prepared using sol gel method. The lattice constant, average grain size and X-ray density are higher for ZCCFO than those of ZNCFO. The magnetic parameters were found to decrease with substitution of Ni by Cu. The maxwell-Wagner's model and Coops theory was used to study the behaviours of imaginary part of permittivity and loss tangent.

J. Mattei et al. worked on electromagnetic properties of composition  $Ni_{0.5}Zn_{0.3}Co_{0.3}Fe_yO_{4-d}$  where y was iron deficient and iron excess and was prepared by chemical co-precipitation. The iron excess sample showed the lower total losses (magnetic and electric) than iron deficient sample TA= 900°C. At frequencies above 700 MHz, the total loss values (IE and ID samples) are prohibitive for antenna downsizing wherever is the firing temperature value (800° C and 900°C). Whereas at frequencies below 700 MHz,  $Ni_{0.5}Zn_{0.3}Co_{0.3}Fe_yO_{4+d}$  may lead to better antenna performances than the  $Ni_{0.5}Zn_{0.3}Co_{0.3}Fe_yO_{4-d}$ .

Palacio Gómez et al. synthesised a set of Nickel-Zinc ferrite samples ( $Ni_{1-x}Zn_xFe_2O_4$ , x = 0.0, 0.2, 0.4, 0.6, 0.8 and 1.0) by the low-energy ball milling method with subsequent thermal treatment. Infrared, Raman and Mössbauer spectroscopies were used to analyze the lattice dynamics and structure of the prepared samples. Infrared studies showed a dominant absorption band ranging from 548  $cm^{-1}$  to 592  $cm^{-1}$  associated with cation-oxygen stretching vibrations at tetrahedral sites. The results obtained are in agreement with those reported in the literature for samples, and the purity of the sample is proved by five Raman modes ( $A_{1g}+E_g+3F_{2g}$ ) observed in the Raman spectra. In  $Ni_{1-x}Zn_xFe_2O_4$  as x increases, the number n of  $Zn_A^{2+}$  ions replacing  $Fe_A^{3+}$  ions at the tetrahedral sites increases and the average super-transferred hyperfine field due to one  $Fe_A^{3+} - O^{2+} - Fe_B^{3+}$  super-exchange interaction was found equal to 0.9 T at 18 K. Finally, the Zn content at tetrahedral sites were calculated from the intensities of the  $A_{1g}$  Raman bands, the relative areas of the A and B sites spectral components in the Mössbauer spectra and from the intensity ratio of certain Bragg peaks ( $I_{(2\ 2\ 0)}/I_{(4\ 4\ 0)}$  and  $(I_{(4\ 0\ 0)}/I_{(2\ 2\ 0)})$  in the

XRD patterns. The values are compared by considering the different approximations required by each technique.

## 2.2 APPLICATIONS OF FERRITES

Ferrites have been immensely used in electronic devices such as home appliances, military communication, equipment and data processing devices. This is because of their important structural, electrical, magnetic properties which are responsible for their applications in various fields due to their technological importance. In High Frequency Devices, the combination of good magnetic properties possessed by ferrites such as high saturation magnetization, electrical properties and high resistivity make ferrite materials suitable as cores for inductors and transformers<sup>52-64</sup>.

In Catalysis, magnetic separation of catalysts in a liquid-phase reaction is much easier than by filtration and centrifugation. Nanostructured magnetically separable catalysts could offer the advantage of their high catalytic efficiency along with easy separation for expensive reactants. Among all the iron oxides, magnetite and hematite are the most common catalysts. In addition catalytic activity of the heterogeneous catalyst with iron oxide has been widely investigated<sup>28,36</sup>.

Medicines: Ferrite nanoparticles hold significant importance in magnetic resonance imaging, magnetic extraction and targeted drug delivery due to good chemical stability and magnetic property. Also, they are used as sealants, lubricants and coolants to the challenging applications in medicine for the purpose of MRI, hyperthermia, targeted drug delivery, biosensors, gene transfer, cell separation and magnetically mediated separation of bio-molecules<sup>17</sup>. These applications require particles that exhibit superparamagnetic behavior at room temperature: that is, they can show magnetic property in the presence of external magnetic field and immediately re-disperse when the magnetic field is removed.

Water Purification: The properties like hierarchical porous structure, narrow sized distribution, large surface area and high magnetization make ferrites very appropriate and stable materials for adsorption of pollutants from waste water. Bulk iron oxide is known to can act as a reducing agent and decompose various toxic chemicals and compound in aqueous solution.

## **CONCLUSION**

Researchers are interested in the synthesis of this ferrite because of its fascinating properties such as the high value of saturation magnetization, low value of coercivity, high initial permeability, narrow size distribution of the ferrite particles, low remanent magnetization, etc. Because of the much better properties they can be used as substituents for other ferrites. Studies have shown that the co-precipitation and sol-gel method are the best for getting the fine crystallite size among all synthesis techniques.

The sol-gel method has been used as an effective alternative to the conventional solid state reaction route for the synthesis of nano-ferrites. It allows for more accurate control over the phase formation, stoichiometry, and particle size uniformity. In the sol-gel method, the particles show homogenous growth with uniform size distribution. SHS offers a fast method for the synthesis of spinel type ferrites with equivalent physical properties to conventional preparations.

Research workers are now giving more preference to the synthesis of nano-scaled ferrite than bulk samples due to their dual-natured magnetic and electrical properties at nanoscale and this is obvious because ferrites at the nano level acquire the distinguishable physical and chemical properties than their bulk forms. These distinguishable and remarkable properties lead to the applicability of ferrites in different fields ranging from the electronics industry to the biomedical field. In recent years, the attention of researchers has increasingly been drawn to the improvement of the synthesis methods in order to obtain the nanoscale spinel materials with improved properties<sup>26</sup>. There is no doubt that the production of quantity ferrite will continue to increase each year, even in the future, as will the advancement of electronic technologies. If researchers and engineers who are concerned with ferrites take a deeper look at the future aspects of ferrites and devote themselves to the subjects of great value, the future of ferrites will experience a steady and more advanced prosperity in science and technology, and their industries will be continue to grow in the future.

## REFERENCES

1. Sugimoto, M. The Past, Present, and Future of Ferrites. *J. Am. Ceram. Soc.* **82**, 269–280 (1999).
2. Poole, C. P., Farach, H. A., Creswick, R. J. & Prozorov, R. Transport Properties. *Superconductivity* **2**, 489–529 (2007).
3. Kumari, N., Kour, S., Singh, G. & Sharma, R. K. A brief review on synthesis, properties and applications of ferrites. *AIP Conf. Proc.* **2220**, 1–5 (2020).
4. Choodamani, C., Nagabhushana, G. P., Rudraswamy, B. & Chandrappa, G. T. Thermal effect on magnetic properties of Mg-Zn ferrite nanoparticles. *Mater. Lett.* **116**, 227–230 (2014).
5. Spiers, H. *et al.* Self propagating high temperature synthesis of magnesium zinc ferrites ( $\text{Mg}_x\text{Zn}_{1-x}\text{Fe}_2\text{O}_3$ ): Thermal imaging and time resolved X-ray diffraction experiments. *J. Mater. Chem.* **14**, 1104–1111 (2004).
6. Nigam, A. & Pawar, S. J. Structural, magnetic, and antimicrobial properties of zinc doped magnesium ferrite for drug delivery applications. *Ceram. Int.* **46**, 4058–4064 (2020).
7. Hajalilou, A. & Mazlan, S. A. A review on preparation techniques for synthesis of nanocrystalline soft magnetic ferrites and investigation on the effects of microstructure features on magnetic properties. *Appl. Phys. A Mater. Sci. Process.* **122**, (2016).
8. Ebrahimi, F., Sajjadi, S. A. & Babakhani, A. On the role of structural variables in magnetic properties of  $\text{Co}_{(1-x)}\text{Ni}_x\text{Fe}_2\text{O}_4$  nanoferrites. *Ceram. Int.* **45**, 20921–20928 (2019).
9. Dippong, T. *et al.* Influence of polyol structure and molecular weight on the shape and properties of  $\text{Ni}_{0.5}\text{Co}_{0.5}\text{Fe}_2\text{O}_4$  nanoparticles obtained by sol-gel synthesis. *Ceram. Int.* **45**, 7458–7467 (2019).
10. Dhiman, P. *et al.* Nanostructured magnetic inverse spinel Ni–Zn ferrite as environmental friendly visible light driven photo-degradation of levofloxacin. *Chem. Eng. Res. Des.* **175**, 85–101 (2021).
11. Su, H., Zhang, H., Tang, X., Jing, Y. & Zhong, Z. Complex permeability and permittivity spectra of polycrystalline Ni-Zn ferrite samples with different microstructures. *J. Alloys Compd.* **481**, 841–844 (2009).
12. Olhero, S. M. *et al.* Co-precipitation of a Ni-Zn ferrite precursor powder: Effects of heat treatment conditions and deagglomeration on the structure and magnetic properties. *J.*

- Eur. Ceram. Soc.* **32**, 2469–2476 (2012).
13. Jiang, N. N. *et al.* Influence of zinc concentration on structure, complex permittivity and permeability of Ni-Zn ferrites at high frequency. *J. Magn. Magn. Mater.* **401**, 370–377 (2016).
  14. Shinde, T. J., Gadkari, A. B. & Vasambekar, P. N. Magnetic properties and cation distribution study of nanocrystalline Ni-Zn ferrites. *J. Magn. Magn. Mater.* **333**, 152–155 (2013).
  15. Jalaly, M., Enayati, M. H., Karimzadeh, F. & Kameli, P. Mechano-synthesis of nanostructured magnetic Ni-Zn ferrite. *Powder Technol.* **193**, 150–153 (2009).
  16. Srinivas, C. *et al.* Study of structural, vibrational, elastic and magnetic properties of uniaxial anisotropic Ni-Zn nanoferrites in the context of cation distribution and magnetocrystalline anisotropy. *J. Alloys Compd.* **873**, 159748 (2021).
  17. Costa, A. C. F. M. *et al.* Influence of calcination temperature on the morphology and magnetic properties of Ni-Zn ferrite applied as an electromagnetic energy absorber. *J. Alloys Compd.* **483**, 563–565 (2009).
  18. Shahane, G. S., Kumar, A., Arora, M., Pant, R. P. & Lal, K. Synthesis and characterization of Ni-Zn ferrite nanoparticles. *J. Magn. Magn. Mater.* **322**, 1015–1019 (2010).
  19. Gabal, M. A., El-Shishtawy, R. M. & Al Angari, Y. M. Structural and magnetic properties of nano-crystalline NiZn ferrites synthesized using egg-white precursor. *J. Magn. Magn. Mater.* **324**, 2258–2264 (2012).
  20. Kumar, S., Kumar, P., Singh, V., Kumar Mandal, U. & Kumar Kotnala, R. Synthesis, characterization and magnetic properties of monodisperse Ni, Zn-ferrite nanocrystals. *J. Magn. Magn. Mater.* **379**, 50–57 (2015).
  21. Džunuzović, A. S. *et al.* Structure and properties of Ni-Zn ferrite obtained by auto-combustion method. *J. Magn. Magn. Mater.* **374**, 245–251 (2015).
  22. Gutiérrez-López, J. *et al.* Microstructure, magnetic and mechanical properties of Ni-Zn ferrites prepared by powder injection moulding. *Powder Technol.* **210**, 29–35 (2011).
  23. Kumbhar, S. S., Mahadik, M. A., Mohite, V. S., Rajpure, K. Y. & Bhosale, C. H. Synthesis and characterization of spray deposited Nickel-Zinc ferrite thin films. *Energy Procedia* **54**, 599–605 (2014).
  24. Yan, W., Jiang, W., Zhang, Q., Li, Y. & Wang, H. Structure and magnetic properties of nickel-zinc ferrite microspheres synthesized by solvothermal method. *Mater. Sci. Eng. B Solid-State Mater. Adv. Technol.* **171**, 144–148 (2010).

25. Deng, N., Zhou, L., Peng, X., Wang, X. & Ge, H. Preparation and characterization of nickel-zinc ferrites by a solvothermal method. *Xiyou Jinshu Cailiao Yu Gongcheng/Rare Met. Mater. Eng.* **44**, 2126–2131 (2015).
26. Luo, H. Y., Yue, Z. X. & Zhou, J. Synthesis and high-frequency magnetic properties of sol-gel derived Ni-Zn ferrite-forsterite composites. *J. Magn. Magn. Mater.* **210**, 104–108 (2000).
27. Rezlescu, N., Rezlescu, L., Popa, P. D. & Rezlescu, E. Influence of additives on the properties of a Ni-Zn ferrite with low Curie point. *J. Magn. Magn. Mater.* **215**, 194–196 (2000).
28. Gul, I. H., Ahmed, W. & Maqsood, A. Electrical and magnetic characterization of nanocrystalline Ni-Zn ferrite synthesis by co-precipitation route. *J. Magn. Magn. Mater.* **320**, 270–275 (2008).
29. Shimada, Y. *et al.* Study on initial permeability of Ni-Zn ferrite films prepared by the spin spray method. *J. Magn. Magn. Mater.* **278**, 256–262 (2004).
30. Zahi, S. Nickel-zinc ferrite fabricated by sol-gel route and application in high-temperature superconducting magnetic energy storage for voltage sag solving. *Mater. Des.* **31**, 1848–1853 (2010).
31. Jadhav, J., Biswas, S., Yadav, A. K., Jha, S. N. & Bhattacharyya, D. Structural and magnetic properties of nanocrystalline Ni[ $\text{sbnd}$ ]Zn ferrites: In the context of cationic distribution. *J. Alloys Compd.* **696**, 28–41 (2017).
32. Hasan, I. H. *et al.* Nickel zinc ferrite thick film with linseed oil as organic vehicle for microwave device applications. *Mater. Chem. Phys.* **236**, 121790 (2019).
33. Kondo, K., Chiba, T. & Yamada, S. Effect of microstructure on magnetic properties of Ni-Zn ferrites. *J. Magn. Magn. Mater.* **254–255**, 541–543 (2003).
34. Wang, L. & Li, F. S. Moessbauer study of nanocrystalline Ni-Zn ferrite. *J. Magn. Magn. Mater.* **223**, 233–237 (2001).
35. Aggarwal, N. & Narang, S. B. Magnetic characterization of Nickel-Zinc spinel ferrites along with their microwave characterization in Ku band. *J. Magn. Magn. Mater.* **513**, 167052 (2020).
36. Lee, S. W. & Kim, C. S. Superparamagnetic properties Ni-Zn ferrite for nano-bio fusion applications. *J. Magn. Magn. Mater.* **304**, 418–420 (2006).
37. Zahi, S., Hashim, M. & Daud, A. R. Synthesis, magnetic properties and microstructure of Ni-Zn ferrite by sol-gel technique. *J. Magn. Magn. Mater.* **308**, 177–182 (2007).
38. Valenzuela, R., Herbst, F. & Ammar, S. Ferromagnetic resonance in Ni-Zn ferrite

- nanoparticles in different aggregation states. *J. Magn. Magn. Mater.* **324**, 3398–3401 (2012).
39. Islam, M. U. *et al.* Electrical behaviour of fine particle, co-precipitation prepared Ni-Zn ferrites. *Solid State Commun.* **130**, 353–356 (2004).
  40. Mangalaraja, R. V., Ananthakumar, S., Manohar, P. & Gnanam, F. D. Initial permeability studies of Ni-Zn ferrites prepared by flash combustion technique. *Mater. Sci. Eng. A* **355**, 320–324 (2003).
  41. Choi, Y., Shim, H. S. & Lee, J. S. Study on magnetic properties and structural analysis of Ni-Zn ferrite prepared through self-propagating high-temperature synthesis reaction by neutron diffractometry. *J. Alloys Compd.* **326**, 56–60 (2001).
  42. Yadoji, P., Peelamedu, R., Agrawal, D. & Roy, R. Microwave sintering of Ni-Zn ferrites: Comparison with conventional sintering. *Mater. Sci. Eng. B Solid-State Mater. Adv. Technol.* **98**, 269–278 (2003).
  43. Khan, K., Maqsood, A., Anis-ur-Rehman, M., Malik, M. A. & Akram, M. Structural, dielectric, and magnetic characterization of nanocrystalline ni-co ferrites. *J. Supercond. Nov. Magn.* **25**, 2707–2711 (2012).
  44. Abdallah, H. M. I., Moyo, T. & Msomi, J. Z. Mössbauer and electrical studies of  $Mn_xCo_{1-x}Fe_2O_4$  compounds prepared via glycothermal route. *J. Supercond. Nov. Magn.* **24**, 669–673 (2011).
  45. Gibin, S. R. & Sivagurunathan, P. Synthesis and characterization of nickel cobalt ferrite ( $Ni_{1-x}Co_xFe_2O_4$ ) nano particles by co-precipitation method with citrate as chelating agent. *J. Mater. Sci. Mater. Electron.* **28**, 1985–1996 (2017).
  46. Niu, Z. P., Wang, Y. & Li, F. S. Magnetic properties of nanocrystalline Co-Ni ferrite. *J. Mater. Sci.* **41**, 5726–5730 (2006).
  47. Choudhary, B. L. *et al.* Irreversible magnetic behavior with temperature variation of  $Ni_{0.5}Co_{0.5}Fe_2O_4$  nanoparticles. *J. Magn. Magn. Mater.* **507**, 166861 (2020).
  48. Mesbahinia, A., Almasi-Kashi, M., Ghasemi, A. & Ramazani, A. FORC investigation of Co-Ni bulk ferrite consolidated by spark plasma sintering technique. *J. Magn. Magn. Mater.* **497**, 165976 (2020).
  49. Abdallah, H. M. I., Moyo, T. & Ngema, N. The effect of temperature on the structure and magnetic properties of  $Co_{0.5}Ni_{0.5}Fe_2O_4$  spinel nanoferrite. *J. Magn. Magn. Mater.* **394**, 223–228 (2015).
  50. Raza Ahmad, M., Jamil, Y., Tabasuum, A. & Hussain, T. Refinement in the structural and magnetic properties of  $Co_{0.5}Ni_{0.5}Fe_2O_4$  and its application as laser micro-

- propellant using ablation confinement. *J. Magn. Magn. Mater.* **384**, 302–307 (2015).
51. Azizi, A., Yoozbashizadeh, H., Yourdkhani, A. & Mohammadi, M. Phase formation and change of magnetic properties in mechanical alloyed  $\text{Ni}_{0.5}\text{Co}_{0.5}\text{Fe}_2\text{O}_4$  by annealing. *J. Magn. Magn. Mater.* **322**, 56–59 (2010).
  52. Shobana, M. K. & Sankar, S. Synthesis and characterization of  $\text{Ni}_{1-x}\text{Co}_x\text{Fe}_2\text{O}_4$  nanoparticles. *J. Magn. Magn. Mater.* **321**, 3132–3137 (2009).
  53. Castrillón Arango, J. A., Cristóbal, A. A., Ramos, C. P., Bercoff, P. G. & Botta, P. M. Mechanochemical synthesis and characterization of nanocrystalline  $\text{Ni}_{1-x}\text{Co}_x\text{Fe}_2\text{O}_4$  ( $0 \leq x \leq 1$ ) ferrites. *J. Alloys Compd.* **811**, (2019).
  54. Ndlovu, B., Msomi, J. Z. & Moyo, T. Mössbauer and electrical studies of  $\text{Ni}_x\text{Co}_{1-x}\text{Fe}_2\text{O}_4$  nanoparticles. *J. Alloys Compd.* **745**, 187–195 (2018).
  55. Chen, B. Y., Chen, D., Kang, Z. T. & Zhang, Y. Z. Preparation and microwave absorption properties of Ni-Co nanoferrites. *J. Alloys Compd.* **618**, 222–226 (2015).
  56. Gao, Y., Zhao, Y., Jiao, Q. & Li, H. Microemulsion-based synthesis of porous Co-Ni ferrite nanorods and their magnetic properties. *J. Alloys Compd.* **555**, 95–100 (2013).
  57. Maqsood, A. & Khan, K. Structural and microwave absorption properties of  $\text{Ni}_{(1-x)}\text{Co}_{(x)}\text{Fe}_2\text{O}_4$  ( $0.0 \leq x \leq 0.5$ ) nanoferrites synthesized via co-precipitation route. *J. Alloys Compd.* **509**, 3393–3397 (2011).
  58. Torkian, S., Ghasemi, A. & Shoja Razavi, R. Cation distribution and magnetic analysis of wideband microwave absorptive  $\text{Co}_x\text{Ni}_{1-x}\text{Fe}_2\text{O}_4$  ferrites. *Ceram. Int.* **43**, 6987–6995 (2017).
  59. Sontu, U. B., G, N. R., Chou, F. C. & M, V. R. R. Temperature dependent and applied field strength dependent magnetic study of cobalt nickel ferrite nano particles: Synthesized by an environmentally benign method. *J. Magn. Magn. Mater.* **452**, 398–406 (2018).
  60. Palacio Gómez, C. A., Barrero Meneses, C. A. & Jaén, J. A. Raman, infrared and Mössbauer spectroscopic studies of solid-state synthesized Ni-Zn ferrites. *J. Magn. Magn. Mater.* **505**, 166710 (2020).
  61. Kim, W. S., Yoon, S. J. & Kim, K. Y. Effects of sintering conditions of sintered NiZn ferrites on properties of electromagnetic wave absorber. *Mater. Lett.* **19**, 149–155 (1994).
  62. Andreev, V. G. *et al.* Influence of microstructure on properties of Ni-Zn ferrite radio-absorbing materials. *J. Magn. Magn. Mater.* **394**, 1–6 (2015).
  63. Thakur, P., Taneja, S., Chahar, D., Ravelo, B. & Thakur, A. Recent advances on

- synthesis, characterization and high frequency applications of Ni-Zn ferrite nanoparticles. *J. Magn. Magn. Mater.* **530**, 167925 (2021).
64. Rezlescu, E., Rezlescu, N., Pasnicu, C., Craus, M. L. & Popa, D. P. The influence of additives on the properties of Ni-Zn ferrite used in magnetic heads. *J. Magn. Magn. Mater.* **117**, 448–454 (1992).
  65. Zhong, Z. *et al.* Synthesis of nanocrystalline Ni-Zn ferrite powders by refluxing method. *Powder Technol.* **155**, 193–195 (2005).
  66. Díaz, A., Valenzuela, R. & Hermosillo, F. A relationship between the globus wall energy and the anisotropy constant in Ni-Zn ferrites. *J. Magn. Magn. Mater.* **15–18**, 1519–1520 (1980).
  67. Ahmed, M. A., El-nimr, M. K., Tawfik, A. & Aboelata, A. M. Dielectric Behaviour in Co-Zn Ferrites. *Phys. Status Solidi* **114**, 377–380 (1989).
  68. Chavan, S. M., Babrekar, M. K., More, S. S. & Jadhav, K. M. Structural and optical properties of nanocrystalline Ni-Zn ferrite thin films. *J. Alloys Compd.* **507**, 21–25 (2010).
  69. Kulikowski, J. & Leśniewski, A. Properties of Ni-Zn ferrites for magnetic heads: Technical possibilities and limitations. *J. Magn. Magn. Mater.* **19**, 117–119 (1980).
  70. Azadmanjiri, J. Structural and electromagnetic properties of Ni-Zn ferrites prepared by sol-gel combustion method. *Mater. Chem. Phys.* **109**, 109–112 (2008).
  71. Mahmud, S. T. *et al.* Influence of microstructure on the complex permeability of spinel type Ni-Zn ferrite. *J. Magn. Magn. Mater.* **305**, 269–274 (2006).
  72. Ramana, P. V., Srinivasa Rao, K. & Rao, K. H. Influence of iron content on the structural and magnetic properties of Ni-Zn ferrite nanoparticles synthesized by PEG assisted sol-gel method. *J. Magn. Magn. Mater.* **465**, 747–755 (2018).
  73. A, E. S. S., Ramana, S., Revathi, B. & Seshagiri, T. 500 007. **57**, 29–37 (1978).
  74. Qin, H. *et al.* Spinel ferrites (MFe<sub>2</sub>O<sub>4</sub>): Synthesis, improvement and catalytic application in environment and energy field. *Adv. Colloid Interface Sci.* **294**, 102486 (2021).
  75. Arai, K. I. & Tsuya, N. Magnetostriction measurements of Ni-Zn ferrite single crystals. *J. Phys. Chem. Solids* **36**, 463–465 (1975).
  76. Bid, S. & Pradhan, S. K. Characterization of crystalline structure of ball-milled nano-Ni-Zn-ferrite by Rietveld method. *Mater. Chem. Phys.* **84**, 291–301 (2004).
  77. Priyadharsini, P., Pradeep, A., Rao, P. S. & Chandrasekaran, G. Structural, spectroscopic and magnetic study of nanocrystalline Ni-Zn ferrites. *Mater. Chem. Phys.* **116**, 207–213 (2009).

78. Montiel, H., Alvarez, G., Gutiérrez, M. P., Zamorano, R. & Valenzuela, R. Microwave absorption in Ni-Zn ferrites through the Curie transition. *J. Alloys Compd.* **369**, 141–143 (2004).
79. Abbas, M., Parvatheeswara Rao, B. & Kim, C. Shape and size-controlled synthesis of Ni Zn ferrite nanoparticles by two different routes. *Mater. Chem. Phys.* **147**, 443–451 (2014).
80. Pan'kov, V. V. & Bashkirov, L. A. Mechanism of NiZn ferrite formation. *J. Solid State Chem.* **39**, 298–308 (1981).
81. Joshi, G. P., Saxena, N. S. & Mangal, R. Temperature dependence of effective thermal conductivity and effective thermal diffusivity of Ni-Zn ferrites. *Acta Mater.* **51**, 2569–2576 (2003).
82. Raghavender, A. T., Biliškov, N. & Skoko, Ž. XRD and IR analysis of nanocrystalline Ni-Zn ferrite synthesized by the sol-gel method. *Mater. Lett.* **65**, 677–680 (2011).
83. Fu, Y. P. & Lin, C. H. Microwave-induced combustion synthesis of Ni-Zn ferrite powder and its characterization. *J. Magn. Magn. Mater.* **251**, 74–79 (2002).
84. Morell, A. Magnetic properties and microstructure of coprecipitated Ni-Zn ferrites sintered by hot-pressing, conventional and fast-firing. *J. Magn. Magn. Mater.* **31–34**, 997–998 (1983).
85. Parvatheeswara Rao, B. P., Caltun, O., Dumitru, I. & Spinu, L. Ferromagnetic resonance parameters of ball-milled Ni-Zn ferrite nanoparticles. *J. Magn. Magn. Mater.* **304**, 752–754 (2006).
86. Satyanarayana, R., Ramana, S., Seshagiri, T. & Rao, S. M. D. (1983) 243-250 243. **90**, 243–250 (1983).
87. Sarangi, P. P., Vadera, S. R., Patra, M. K. & Ghosh, N. N. Synthesis and characterization of pure single phase Ni-Zn ferrite nanopowders by oxalate based precursor method. *Powder Technol.* **203**, 348–353 (2010).
88. Wang, H. W. & Kung, S. C. Crystallization of nanosized Ni-Zn ferrite powders prepared by hydrothermal method. *J. Magn. Magn. Mater.* **270**, 230–236 (2004).
89. Haque, M. M., Maria, K. H., Choudhury, S., Bhuiyan, M. A. & Hakim, M. A. Synthesis, microstructure and magnetic properties of Ni-Mg ferrites. *J. Ceram. Process. Res.* **14**, 82–86 (2013).
90. Chaudhari, N. D., Kambale, R. C., Bhosale, D. N., Suryavanshi, S. S. & Sawant, S. R. Thermal hysteresis and domain states in Ni-Zn ferrites synthesized by oxalate precursor method. *J. Magn. Magn. Mater.* **322**, 1999–2005 (2010).

91. Thomas, J. J., Shinde, A. B., Krishna, P. S. R. & Kalarikkal, N. Cation distribution and micro level magnetic alignments in the nanosized nickel zinc ferrite. *J. Alloys Compd.* **546**, 77–83 (2013).
92. Safari, A., Gheisari, K. & Farbod, M. Structural, microstructural, magnetic and dielectric properties of Ni-Zn ferrite powders synthesized by plasma arc discharge process followed by post-annealing. *J. Magn. Magn. Mater.* **488**, 165369 (2019).

